Effect of hydraulic retention time on the electro-bioremediation of nitrate in saline groundwater

Giulia Puggioni[1,2], Stefano Milia[*,3], Valentina Unali[3], Riccardo Ardu[1,4], Elena Tamburini[4], M. Dolors Balaguer[2], Narcìs Pous[2], Alessandra Carucci[1,3], Sebastià Puig[2]

[1] University of Cagliari – Department of Civil-Environmental Engineering and Architecture (DICAAR), Via Marengo 2 - 09123, Cagliari, Italy

[2] Laboratory of Chemical and Environmental Engineering (LEQUiA), Institute of the Environment, University of Girona, Carrer Maria Aurelia Capmany, 69, E-17003 Girona, Spain

[3] National Research Council of Italy - Institute of Environmental Geology and Geoengineering (CNR-IGAG), Via Marengo 2 - 09123, Cagliari, Italy

[4] DiSB, Department of Biomedical Sciences, University of Cagliari, Cittadella universitaria, 09042 Monserrato (CA), Italy

[*] Corresponding author:

E-mail address: stefano.milia@igag.cnr.it

National Research Council of Italy - Institute of Environmental Geology and Geoengineering (CNR-IGAG), Via Marengo 2 - 09123, Cagliari, Italy

Tel. +39 070 675 5517, Fax +39 070 675 5523

Abstract:

Bioelectrochemical systems (BES) have proven their capability to treat nitrate-contaminated saline groundwater and simultaneously recover value-added chemicals (such as disinfection products) within a circular economy-based approach. In this study, the effect of the hydraulic retention time (HRT) on nitrate and salinity removal, as well as on free chlorine production, was investigated in a 3-compartment BES working in galvanostatic mode with the perspective of process intensification and future scale-up. Reducing the HRT from 30.1±2.3 to 2.4±0.2 hours led to a corresponding increase in nitrate removal rates (from 17±1 up to

131±1 mgNO_3^--N $L^{-1}d^{-1}$), although a progressive decrease in desalination efficiency (from 77±13 to 12±2%) was observed. Nitrate concentration and salinity close to threshold limits indicated by the World Health Organization for drinking water, as well as significant chlorine production were achieved with an HRT of 4.9±0.4 h. At such HRT, specific energy consumption was low ($6.8 \cdot 10^{-2} \pm 0.3 \cdot 10^{-2}$ kWh $g^{-1}NO_3^-N_{removed}$), considering that the supplied energy supports three processes simultaneously. A logarithmic equation correlated well with nitrate removal rates at the applied HRTs and may be used to predict BES behaviour with different HRTs. The bacterial community of the bio-cathode under galvanostatic mode was dominated by a few populations, including the genera *Rhizobium, Bosea*, *Fontibacter* and *Gordonia*. The results provide useful information for the scale-up of BES treating multi-contaminated groundwater.

Keywords: circular economy; denitrification; microbial electrochemical technology; saline groundwater; value-added products; water recovery.

1. INTRODUCTION

Groundwater is a critical freshwater reservoir, fundamental for global water and food security. Since the spread of contaminants in groundwater can limit its use as drinking water, actions must be taken to ensure its safe supply (Janža, 2022). Bioelectrochemical systems (BES) have emerged as sustainable alternatives to conventional bioremediation technologies for treating contaminated groundwater. Such systems are based on the ability of electroactive microorganisms to perform oxidation and reduction reactions by exchanging electrons with an electrode (Pous et al., 2018; Wang et al., 2020). Therefore, they are particularly suitable for groundwater treatment, as they promote bioremediation without needing chemicals as electron acceptors/donors.

Since groundwater may be simultaneously exposed to different sources of pollution, one of the most intriguing challenges that researchers are currently facing is the application of BES to the bioremediation of multi-contaminated groundwater (Ceballos-Escalera et al., 2021; Wang et al., 2021; Cruz Viggi et al., 2022; Tucci et al., 2021, Puggioni et al., 2021). Among contaminants, nitrate is often found in groundwater due to inefficient farming practices and careless management of livestock activities (Kwon et al., 2021; Serio et al., 2018), thus hindering the exploitation of such important water reservoirs since it is related to severe health risks (Carrey et al., 2021; Ward et al., 2018). BES proved to be a promising solution for the remediation of nitrate-contaminated groundwater (Li et al., 2019; Pous et al., 2018), and they have demonstrated the possibility of achieving complete nitrate conversion into dinitrogen gas via autotrophic denitrification at the bio-cathode, with no or negligible production of intermediates such as nitrite and nitrous oxide (Ceballos-Escalera et al. 2021; Puig et al. 2011; Desloover et al., 2011).

Besides nitrates, the occurrence of salinity in groundwater is often related to the over-exploitation of water reservoirs in coastal areas, which causes the alteration of the hydrodynamic balance between seawater and freshwater. The consequent seawater intrusion and salinisation of the aquifer limit the potential use of groundwater for human consumption (Liu et al., 2020). BES-based desalination through Microbial Desalination Cells (MDC) has been successfully applied, especially for seawater desalination. In such systems, the electric potential gradient created by the exoelectrogenic bacteria in the presence of organic matter allows water desalination by driving ion transport through a series of ion-exchange membranes (Ramírez-Moreno et al., 2019; Sevda et al., 2015; Kim et al., 2013).

Though the combination of high nitrate concentrations and salinity levels severely affects groundwater quality in many countries worldwide (Troudi et al., 2020; Alfarrah et al., 2018;

Gounari et al., 2014), only a few studies concerning their simultaneous removal using BES have been reported in the literature so far. Zhang et al. (2013) successfully tested a 2-compartment submerged microbial desalination-denitrification cell (SMDDC) for the treatment of synthetic groundwater affected by high salinity and nitrate concentration (0.9-2.2 mS cm^{-1} and 20 mgNO_3^--N L^{-1}, respectively). A readily degradable organic substrate (i.e., sodium acetate, 800 mg L^{-1}) was spiked in the anode to sustain the process. The system achieved salinity and nitrate removal efficiencies of up to 60% and 99%, respectively, at the highest ionic strength tested. Recently, our research group designed and tested a proof-of-concept configuration based on a 3-compartment BES for the simultaneous removal of nitrate (30 mgNO_3^--N L^{-1}) and salinity (3.3±0.3 mS cm^{-1}) from synthetic saline groundwater, without any addition of organic substrates, and with the concomitant production of a value-added chemical (i.e., free chlorine, a disinfectant commonly used in water and wastewater treatment plants) (Puggioni et al., 2021). In this reactor, the electroactive biofilm attached to the bio-cathode carried out full autotrophic denitrification. At the same time, desalination took place in the central compartment thanks to the electrochemically driven migration of ions across two ion-exchange membranes. Part of the accumulated chloride was converted into chlorine in the anode compartment. Different operating strategies were tested, and the galvanostatic operation (applied current, 10 mA) with pH control (< 9) in the bio-cathode compartment resulted in high nitrogen and salinity removal efficiencies (69±2% and 63±5%, respectively) and significant recovery of free chlorine. Standard quality requirements for drinking water in terms of nitrate concentration (91/767/EU, 11.3 mgNO_3^--N L^{-1}) and electrical conductivity (98/83/CE, 2.5 mS cm^{-1}) were successfully met at high hydraulic retention time (HRT) with no apparent limitations to biological nor physical-chemical processes involved. The proposed 3-compartment

configuration still showed ample room for improvement in terms of nitrate removal rates and specific energy consumption.

Among the operating parameters that can optimise the process, the HRT is known to influence denitrifying BES performance, which can be severely limited by the hydrodynamics and the corresponding distribution of nitrate/substrates in the system (Vilà-Rovira et al., 2015). Pous et al. (2015) reported that insufficient mixing could generate different gradients of nitrate and pH along the reactor, producing different environments and, thus, heterogeneity in microbial growth and activity. Ceballos-Escalera et al. (2021) observed an increase in nitrate removal rates (from 166±22 to 247±22 $mgNO_3^-$-N $L^{-1}d^{-1}$) as the HRT was progressively reduced from 7.5±0.2 to 3.6±0.2 h in a tubular BES treating synthetic nitrate- and arsenic-contaminated groundwater (28±6 $mgNO_3^-$-N L^{-1} and 5 mgAs(III) L^{-1}, respectively). Pous et al. (2017) observed the enhancement of nitrate removal rates (from 73±5 to 849±23 $mgNO_3^-$-N $L^{-1}d^{-1}$) with decreasing HRTs (from 10.89±0 to 0.46±0.01 h) in a tubular BES fed with synthetic nitrate-contaminated groundwater (33 $mgNO_3^-$-N L^{-1}). Such behaviour was mainly attributed to the increase in bacterial activity rather than bacterial growth due to the reinforced water flowrate itself, and not due to the increase in nitrate availability (Pous et al., 2017). However, short HRT has been proved to have a detrimental effect on desalination technologies such as microbial desalination cells since it negatively influences biomass activities at the anode (Imoro et al., 2021) and current generation (Jingyu et al., 2017).

Within this framework, the influence of the HRT on denitrification and desalination performance of the 3-compartment cell configuration developed by Puggioni et al. (2021) was investigated in this study. Since the overall effect of decreasing HRT is difficult to be predicted when biotic (e.g., nitrate removal) and abiotic (i.e., desalination, chloride removal

and chlorine production) processes co-exist in the same reactor, the outcomes of this study will provide helpful information for maximising system's performance and finding its operational limits, with the perspective of fostering the scale-up of the system by reducing the capital and operating costs linked to the size of the reactors and the energy consumption, respectively.

2. MATERIALS AND METHODS

2.1 Reactor set-up

Two identical 3-compartment cells made of polycarbonate were used (Puggioni et al., 2021). Each cell consisted of a bio-cathode compartment (8x8x2 cm^3, net volume 110±9 mL), an anode compartment (8x8x2 cm^3, net volume 130±7 mL), and a thin central desalination compartment (8x8x0.5 cm^3, net volume 31±2 mL). Such a peculiar geometric configuration was designed to minimise the distance between the electrodes and the membranes and consequently decrease the internal resistance of the system. The bio-cathode compartment contained the graphite felt electrode (64 cm^2, degree of purity 99.9%, AlfaAesar, Germany), and it was physically separated from the central compartment by a cation exchange membrane (CEM 7000, Membrane International Inc., USA). The anode compartment, containing a titanium mesh electrode coated with mixed metals oxide (Ti-MMO, 15 cm^2, NMT-Electrodes, South Africa), was physically separated from the central compartment by an anion exchange membrane (AEM 7001, Membranes International Inc., USA). A reference electrode (Ag/AgCl, +0.197 V vs SHE, mod. MF2052, BioAnalytical Systems, USA) was placed in the bio-cathode compartment. Cathode, anode, and reference electrodes were connected to a multichannel potentiostat (Ivium technologies, IviumNstat, NL). The system was thermostatically controlled at 25±1 °C.

2.2 Groundwater characteristics

A synthetic medium mimicking nitrate concentration and salinity of groundwater from the nitrate vulnerable zone of Arborea (Sardinia, Italy) was fed to the bio-cathode compartment. This medium contained 216.6 mg L^{-1} KNO_3 (corresponding to 30.0 mgNO_3^--N L^{-1}); 10 mg L^{-1} NH_4Cl (corresponding to 2.6 mgNH_4^+-N L^{-1}), 4.64 mg L^{-1} KH_2PO_4; 11.52 mg L^{-1} K_2HPO_4; 350 mg L^{-1} $NaHCO_3$; 2000 mg L^{-1} NaCl and 100 µL L^{-1} of trace elements solution (Patil et al., 2010). The resulting electrical conductivity and pH were 3.06±0.5 mS cm^{-1} and 8.2±0.3, respectively. The medium was prepared using distilled water and pre-flushed with N_2 gas for 15 minutes to avoid any presence of oxygen.

2.3 Experimental procedure

The cells were already running from previous research, and the initial inoculum consisted of the supernatant of activated sludge liquor drawn from the municipal wastewater treatment plant of Cagliari (Italy) and the effluent from a parent electro-denitrifying system in a 60:40 (v:v) mixture (Puggioni et al., 2021). The bio-cathode compartment was continuously fed with groundwater, and the effluent was sent into the central compartment to achieve desalination. The anode compartment was filled with tap water (Pous et al., 2015) to minimise the use of chemicals and operated in batch mode with recirculation. Tap water was periodically replaced (about every 10 days) to avoid excessive chlorine accumulation. According to the best operating strategy defined in Puggioni et al. (2021), the potentiostat was set in galvanostatic mode at a current of 10 mA (0.16 mA $cm^{-2}_{membrane}$), and pH control (< 9) was implemented to avoid excessive pH increase in the bio-cathode compartment, by dosing HCl (1 M) in the bio-cathode recirculation line. The probe for continuous pH measurement (Mettler Toledo, mod. InPro 3253i/SG/225, USA) was connected to a transmitter (Mettler Toledo, mod. M300, USA), which recorded data every 10 minutes.

Since the enhancement of electro-bioremediation systems must be linked to the treatment capacity, the HRT was used as the operational parameter, as summarised in Table 1. Each HRT was maintained for about one month with constant nitrate influent concentration (29.3±3.5 mgNO_3^--N L^{-1}).

Table 1. Experimental procedure.

Tests	**Q_{inf}** [L d^{-1}]	**HRT*** [h]	**HRT_{des}**** [h]	**NO_3^--N loading rate** [mg L^{-1} d^{-1}]
1	0.11	30.1±2.3	6.7±0.3	23.57±1.84
2	0.17	20.3±1.5	4.5±0.2	35.14±2.39
3	0.31	10.9±0.8	2.4±0.1	62.61±3.90
4	0.46	7.3±0.6	1.6±0.1	82.21±3.07
5	0.68	4.9±0.4	1.1±0.05	125.48±2.98
6	1.42	2.4±0.2	0.5±0.02	261.05±16.07
7	0.68	4.9±0.4	1.1±0.05	130.92±11.27

* calculated considering the sum of volumes of the bio-cathode and central compartments.

** calculated considering the volume of the central compartment.

In particular, Test 7 was implemented as a repetition of Test 5 to restore process performance after observing the worsening of denitrification activity in Test 6. Hence, the results achieved during Test 7 were not included in graphical representations nor in the calculations to make the results easier to interpret.

2.4 Analytical methods

Samples were periodically drawn from influent (once per week), effluent (three times per week), bio-cathode and anode compartments (three times per week) in order to evaluate overall cell performances. The same samples from the duplicate cell were taken once a week to confirm the process progress of the main cell. Liquid samples were analysed for quantification of anions, i.e., chloride (Cl^-), nitrite (NO_2^--N), nitrate (NO_3^--N), phosphate (PO_4^{3-}), and sulphate (SO_4^{2-}), using an ion chromatograph (ICS-90, Dionex-Thermofisher,

USA) equipped with an AS14A Ion-PAC 5 μm column. Samples were filtered (acetate membrane filter, 0.45 μm porosity) and properly diluted with grade II water. The concentrations of the main cations, i.e., potassium (K^+) and sodium (Na^+), were determined using an ICP/OES (Varian 710-ES, Agilent Technologies, USA): samples were filtered (acetate membrane filter, 0.45 μm porosity), acidified (nitric acid, 1% v:v) and diluted with grade I water.

Electrical conductivity and pH were measured using a benchtop meter (HI5522, Hanna Instruments, Italy).

The concentration of free chlorine was analysed using spectrophotometric techniques (DR1900, Hach Lange, Germany) and the DPD (N,N-diethyl-p-phenylenediamine) free chlorine method (DPD free chlorine reagent powder pillows Cat. 2105569, Hach Lange, Germany).

Nitrous oxide (N_2O) was measured using an N_2O liquid-phase microsensor (Unisense, Denmark) located in the effluent line of the reactors, thanks to a dedicated glass measuring cell. The resulting bio-cathode potentials were recorded every five minutes through the potentiostat (Ivium technologies, IviumNstat, NL). Cell potential was periodically checked using a multimeter (K2M, mod. KDM-600C, Italy).

2.5 Calculations

Nitrate Removal Efficiency (N-RE) and Nitrate Removal Rate (N-RR) were calculated according to equations 1 and 2, respectively:

$$N - RE\ [\%] = \frac{C_{NO_3^- - N(inf)} - C_{NO_3^- - N(eff)}}{C_{NO_3^- - N(inf)}} \times 100 \qquad \textbf{(1)}$$

$$N - RR\ [mg\ N\ L^{-1}\ d^{-1}] = \frac{C_{NO_3^- - N(inf)} - C_{NO_3^- - N(eff)}}{HRT} \qquad \textbf{(2)}$$

Where $C_{NO3^-N(inf)}$ and $C_{NO3^-N(eff)}$ [$mgNO_3^-N\ L^{-1}$] are nitrate concentrations in the influent and the effluent, respectively, while *HRT* [d] is the hydraulic retention time considering the volumes of the cathodic and central compartments.

The desalination performance was evaluated by calculating the electrical conductivity removal efficiency (EC-RE, equation 3), the chloride removal efficiency (Cl^--RE, equation 4), and the chloride removal rate (Cl^--RR, equation 5).

$$EC - RE\ [\%] = \frac{EC_{(inf)} - EC_{(eff)}}{EC_{(inf)}} \times 100 \quad \textbf{(3)}$$

$$Cl^- - RE\ [\%] = \frac{C_{Cl^-(inf)} - C_{Cl^-(eff)}}{C_{Cl^-(inf)}} \times 100 \quad \textbf{(4)}$$

$$Cl^- - RR\ [mg\ L^{-1}\ d^{-1}] = \frac{C_{Cl^-(inf)} - C_{Cl^-(eff)}}{HRT_{des}} \quad \textbf{(5)}$$

where $EC_{(eff)}$ [$mS\ cm^{-1}$] and $C_{Cl^-(eff)}$ [$mg\ L^{-1}$] represent the effluent electrical conductivity and chloride concentration, respectively. $EC_{(inf)}$ and $C_{Cl^-(inf)}$ correspond to the electrical conductivity and chloride concentration of the solution in the bio-cathode compartment (i.e., the influent to the central compartment), respectively, to consider the chloride input due to the acid dosage in this compartment. HRT_{des} [d] is the hydraulic retention time of the central compartment.

The coulombic efficiency for nitrate reduction (εNO_x) was calculated according to equation 6 (Virdis et al., 2008):

$$\varepsilon NO_x[\%] = \frac{I}{n\,\Delta C_{NO_x} Q_{inf} F} \times 100 \quad \textbf{(6)}$$

where *I* is the fixed current [A]; *n* is the number of electrons that can be accepted by 1 mol of oxidised nitrogen compounds present in the bio-cathode compartment, assuming N_2 is the final product; ΔC_{NOx} is the difference between the nitrate concentration in the cathodic influent and effluent [$molNO_3^-N\ L^{-1}$]; Q_{inf} is the influent flowrate [$L\ s^{-1}$]; *F* is Faraday's constant [96485 $Ce^-\ mol^{-1}$].

The current efficiency (CE) was expressed as the percentage of the charge associated with the chloride removed from the central compartment to the amount of electric charge transferred (ECT) across the membranes (Ramírez-Moreno et al., 2019). CE [%] and ECT [C m^{-3}] were calculated using equations 7 and 8, respectively:

$$CE\ [\%] = \frac{v\ z\ F\left(C_{Cl^-(inf)} - C_{Cl^-(eff)}\right)}{ECT} \times 100 \quad \textbf{(7)}$$

$$ECT\ [C\ m^{-3}] = \frac{\int I\ dt}{V} \quad \textbf{(8)}$$

where *v* and *z* represent the stoichiometric coefficient and the valence of the chloride ion, respectively; *V* [m^{-3}] is the volume of water treated; *dt* is the time [s].

The specific energy consumption (SEC) was calculated according to equation 9 (Jingyu et al., 2017):

$$SEC\ [kWh\ m^{-3}] = \frac{I \int E\ dt}{V} \quad \textbf{(9)}$$

where *E* is the cell potential [V].

2.6 Analysis of bacterial community by NGS of 16S rRNA gene

The composition of the bacterial community in the cathodic biofilm was characterised. Samples of the biofilms formed on the bio-cathode were axenically collected during Test 5 (Table 1). Five cathode points were sampled, and the biomass was pooled into a composite sample to mitigate the effects of microscale heterogeneity on the bio-cathode. Biomass samples were stored at -20°C before DNA extraction. Genomic DNA was extracted from biomass samples (250 mg wet weight) using the DNeasy PowerSoil Pro Kit (QIAGEN), and DNA was subsequently purified using the DNeasy PowerClean Cleanup Kit (QIAGEN). The DNA quality and concentration were determined on agarose gel using a DNA quantitation standard. DNA samples were submitted to Bio-Fab Research Srl (Rome, Italy) for sequencing of the V3-V4 region of the bacterial 16S rRNA gene on an Illumina Miseq

platform (Illumina, San Diego, CA) using 2 × 300 bp paired-end reads. The primer pair was used S-D-Bact-0341-b-S-17/S-D-Bact-0785-a-A-21 (Klindworth et al., 2013).

For data processing, raw sequences were demultiplexed by the sequencing facility. Reads were trimmed to remove primer sequences using the CutAdapt version 3.5. Sequences were imported into Quantitative Insights into Microbial Ecology (QIIME 2) version 2020-11 (Bolyen et al., 2019). Using the DADA2 pipeline (Callahan et al., 2016), reads with ambiguous and poor-quality bases were discarded, good-quality reads dereplicated and denoised, and the paired reads merged. Chimeras and singletons were identified and removed from the dataset. DADA2 was used to produce alternative sequence variants (ASVs), thus obtaining a filtered ASV-abundance table. For each ASV, a representative sequence was used for taxonomy assignment against the Silva database release 138 (Quast et al., 2013). Richness was estimated as the number of observed ASV by using the vegan R package (Oksanen et al., 2019). Read count data were normalised by Cumulative Sum Scaling (CSS) transformation using the metagenomeSeq package (Paulson et al., 2013). The Bray-Curtis similarity index between samples was calculated.

3. RESULTS AND DISCUSSION

3.1 Effect of the HRT on denitrification and desalination performances

The system's enhancement was tested by increasing the influent flowrate and, thus, reducing the HRT. Figure 1 shows the average NO_3^--N loading and removal rates (N-LR and N-RR, respectively) at different influent flowrates.

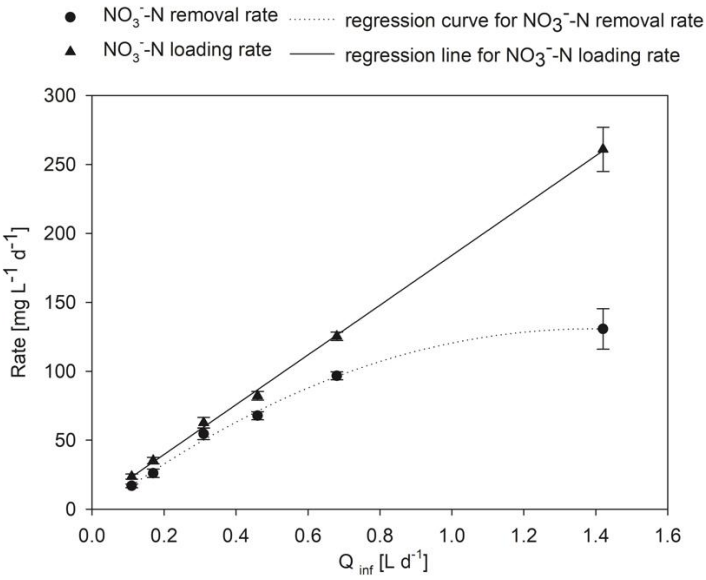

Figure 1. Average trend in N-LR and N-RR with increasing influent flowrates (Q_{inf}).

The N-LR was increased from 23.6±1.8 mgNO_3^--N $L^{-1}d^{-1}$ (Test 1) to 261±16 mgNO_3^--N $L^{-1}d^{-1}$ (Test 6), and the N-RR increased as well (from 16.9±1.3 mgNO_3^--N $L^{-1}d^{-1}$ to 130.8±14.7 mgNO_3^--N $L^{-1}d^{-1}$), though it did not follow the same linear trend as the N-LR. Such an increase in the N-RR was likely ascribed to improved hydrodynamics conditions which minimised the occurrence of nitrate and pH gradients in the bio-cathode compartment, with the corresponding increase in the denitrifying activity (Pous et al., 2017; Vilà-Rovira et al., 2015). The increase in nitrate removal rate with decreasing HRT was also observed in previous studies. Figure 2 compares the trend of N-RR versus the HRT observed in the current study with those reported by Pous et al. (2017) and Ceballos-Escalera et al. (2021), exploiting tubular systems with hydraulically connected anode and cathode compartments. Although the systems were highly heterogeneous in terms of configuration (3-chamber plate cell vs tubular cells), electrode materials (graphite felt vs granular graphite), and operating conditions (galvanostatic vs potentiostatic modes), the same mathematical model was able to fit the observed N-RR vs HRT relationship.

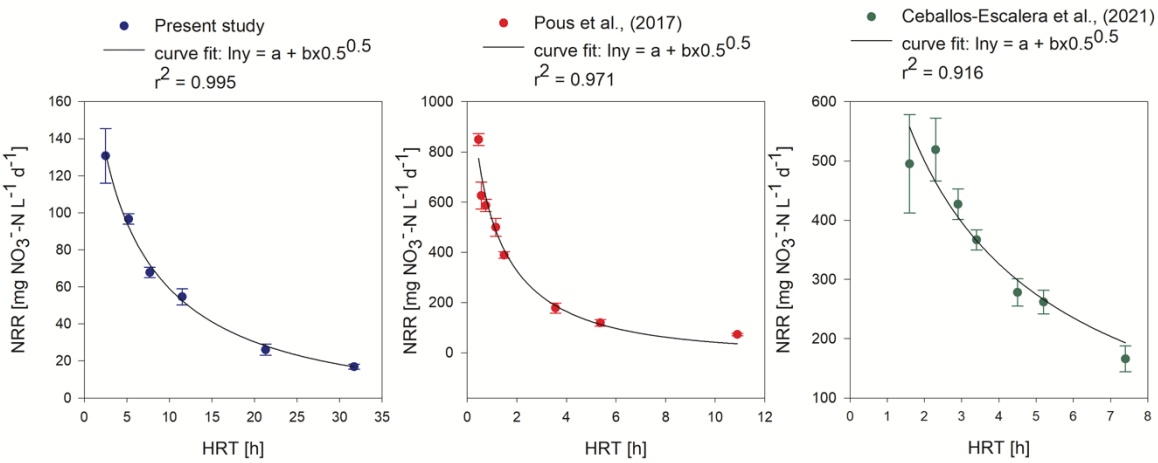

Figure 2. Comparison of nitrate removal rate (N-RR) trend versus the HRT observed in the present study with those reported by Pous et al. (2017) and Ceballos-Escalera et al. (2021), and modelling of results.

This result is interesting as it proves that, regardless of the type of configuration or operating conditions used, the process behaviour with different HRTs may be reasonably predicted, providing useful information in the perspective of reactor scale-up.

Despite the increasing N-RR observed in our study with decreasing HRT, nitrate concentration in the effluent started to increase from Test 4 onward (Figure 3). However, it remained below the threshold level of 11.3 mgNO_3^--N L^{-1} (Nitrate Directive 91/767/EU) throughout the experiment except during Test 6 (Q_{inf}, 1.42 L d^{-1}; HRT, 2.4±0.2 h), when an average concentration of 13.5±2.8 mgNO_3^--N L^{-1} (corresponding to an N-RE of 50±8%) was observed. Since the applied current was initially much higher than that theoretically required to remove the nitrate input (10 mA applied vs approx. 1.4 mA theoretically required in Test 1), the coulombic efficiency for nitrate removal was always above 100%, decreasing as the HRT decreased, and reaching values close to 100% during Test 6.

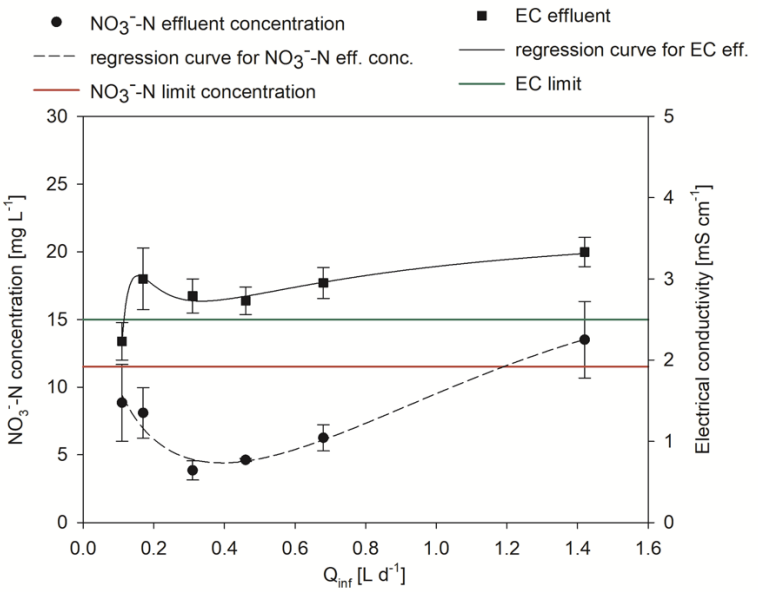

Figure 3. Trends of average NO_3^--N concentration and electrical conductivity (EC) in the effluent with increasing Q_{inf}.

During Test 6, nitrite and nitrous oxide were detected in the effluent at low concentrations (0.22±0.08 mgNO_2^--N L^{-1} and up to 0.5 mgN_2O-N L^{-1}, respectively). Pous et al. (2013) observed the formation of such stable intermediates in a denitrifying MFC treating groundwater, and their presence was linked to reduced bacterial NO_2^-- and N_2O-reduction activities due to a change in the operating conditions (in that case, the influent composition). Virdis et al. (2009) observed lower N_2O reduction rates in an MFC performing carbon and nitrogen removal, compared to NO_3^- reduction rates. Further tests suggested a possible limitation through which the cathodic biofilm was not able to reduce N_2O at the same rate as it was produced by the previous step of denitrification. In our study, the further increase in nitrate removal rate observed in Test 6 was not fully accompanied by a corresponding increase in nitrite and nitrous oxide removal rate, but still, 97% of NO_3^- removed was converted into N_2. Such behaviour was related to the worsening of the denitrification process, therefore process boundary conditions were considered to lie in an HRT range between approximately 5 h (Test 5) and 2.5 h (Test 6).

A final test (Test 7) was carried out setting the same HRT as Test 5 (i.e., 4.9±0.4 h) to restore the denitrifying process and verify microbial activity. The performance in terms of nitrate removal observed during Test 5 (N-RE = 77±3% and N-RR = 96.7±2.8 mgNO_3^--N $L^{-1}d^{-1}$) was immediately restored during Test 7 (N-RE = 89±4% and N-RR = 112±7.5 mgNO_3^--N $L^{-1}d^{-1}$), and the average effluent NO_3^--N concentration was 3±1 mgNO_3^--N L^{-1}, far below the threshold limit for drinking water. No nitrite or nitrous oxide were detected in the effluent during Test 7, indicating that the worsening of nitrate removal with the production of intermediates observed during Test 6 was reversible. The slight increase in process performance observed between Test 5 and Test 7 demonstrates that biomass growth may have played a small role in improving the denitrification rates.

An almost opposite behaviour was observed for the desalination process. The best performance was observed during Test 1 when the average effluent conductivity was 2.2±0.2 mS cm^{-1}, below the threshold level of 2.5 mS cm^{-1} (98/83/CE Directive) (Figure 3). Figure 4 shows the trend of electrical conductivity in the influent and effluent of the central desalination compartment and the corresponding desalination efficiency (EC-RE). The decrease in overall EC-RE with decreasing HRT due to the reduced contact time was counterbalanced by the higher amount of influent treated per day. As expected, the overall conductivity removal rate did not vary substantially throughout the experiment (23.4±7.3 mS $cm^{-1}d^{-1}$). In fact, the salinity of simulated groundwater in our study was primarily related to different ions rather than nitrate (e.g., chloride, sodium, etc.), and desalination was mostly relying on physicochemical separation and electromigration rather than biological removal. Though the precipitation of cations such as Ca^{2+} and Mg^{2+} at high concentrations led to reduced power generation and desalination efficiency in MDCs treating saltwater and seawater (Luo et al., 2012; Rahman et al., 2021), much lower ions concentrations were involved in our study. Therefore the possible effects of ion precipitation on membrane

ion-exchange capacity and overall desalination performance are reasonably expected to be much less significant, thus allowing a longer lifespan for the membranes. To enhance salinity removal and keep the conductivity below threshold levels, a valuable operating strategy may consist in increasing the applied current proportionally with the increase in influent flowrate.

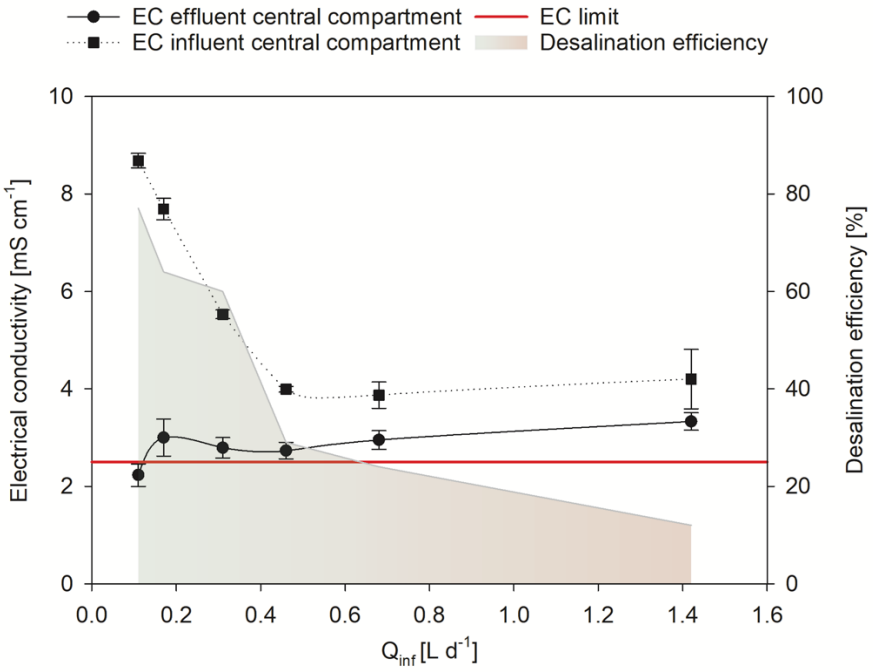

Figure 4. Average trend of central compartment influent and effluent electrical conductivity, and desalination efficiency versus the influent flowrate. The red line indicates the threshold limit for the electrical conductivity in freshwater (2.5 mS cm^{-1}).

The influent conductivity of the central desalination compartment (corresponding to the effluent of the bio-cathode compartment) dropped from 8.7±0.2 mS cm^{-1} (Test 1) to 4.2±0.6 mS cm^{-1} (Test 6), likely as a result of the increased influent flowrate which probably led to a faster turnover of the solution in the bio-cathode compartment, thus reducing the accumulation of chlorides dosed as HCl for pH control, and cations migrating from the central compartment through the CEM. The average chloride concentration measured in the cathode chamber (including the contribution of HCl dosage) decreased from 3622±443 (Test 1) to 1385±56 $mgCl^{-}$ L^{-1} (Test 6), while sodium concentration decreased from 2355±370 to 1040±182 $mgNa^{+}$ L^{-1}.

On the other hand, the effluent electrical conductivity slightly increased to 3.3 mS cm^{-1}, resulting in the reduction of the overall desalination efficiency, which dropped from 77±13% (Test 1) to 12±2% (Test 6). Coherently, the current efficiency related to the removal of chloride in the central compartment decreased from 89±14% (Test 1) to 59±15% (Test 6). Such behaviour was related to the increase in the influent flowrate which resulted in too low HRT_{des} (from 6.7±0.3 h in Test 1 to 0.5±0.02 h in Test 6). The theoretical quantity of chloride ions that can be transferred through the membranes by applying a current of 10 mA at the different HRT tested ranges from 2.8 g L^{-1} (Test 1) to 0.22 g L^{-1} (Test 6), very close to those actually observed (i.e., 2.5±0.4 and 0.13±0.03 $gCl^-_{removed}$ L^{-1} in Tests 1 and 6, respectively). Thus, the HRT decrease did not allow sufficient ions to migrate through the membranes to observe a significant reduction in effluent electrical conductivity. The adverse effect of low HRT on desalination performance was already demonstrated for MDCs by Jingyu et al. (2017), who reported that reducing the HRT leads to lower current generation and, consequently, to lower removal of total dissolved solids (TDS).

Chlorine production in the anode compartment was monitored throughout the whole experimentation. An essential aspect of process monitoring is the durability of materials in contact with chlorine, as it is a powerful oxidant which may damage them. For this reason, it was decided to replace the solution in the anodic chamber periodically (about every 10 days, resulting in an average concentration of 16±1 $mgCl_2$ L^{-1}). Higher values of chlorine concentration (i.e., approximately 30 $mgCl_2$ L^{-1}) were obtained by Puggioni et al. (2021) without the periodic replacement of the solution, resulting in damage of reactors' materials.

3.2 Considerations on pH evolution during the process

Increasing the influent flowrate also affected the pH trend in the different compartments. pH control plays a significant role in ensuring optimal denitrifying microbial activity, as a neutral pH is strictly necessary for this biological process (Clauwaert et al., 2009). Such

control has become essential to optimise water desalination performance. Several studies demonstrated that the pH gradient between the anode and cathode compartments could lead to potential losses (Puig et al., 2012) that adversely affect the desalination efficiencies of MDCs (Jingyu et al., 2017).

During the whole experiment, the periodic dosage of acid to control the pH in the bio-cathode compartment remained constant. This resulted in a difference mainly in the effluent pH as a function of the influent flowrate. As shown in Figure 5, while the influent pH remained almost constant, the effluent pH increased from near-acidic (i.e., 4.1±1.2 in Test 1) to slightly alkaline (i.e., 7.8±0.3 in Test 6).

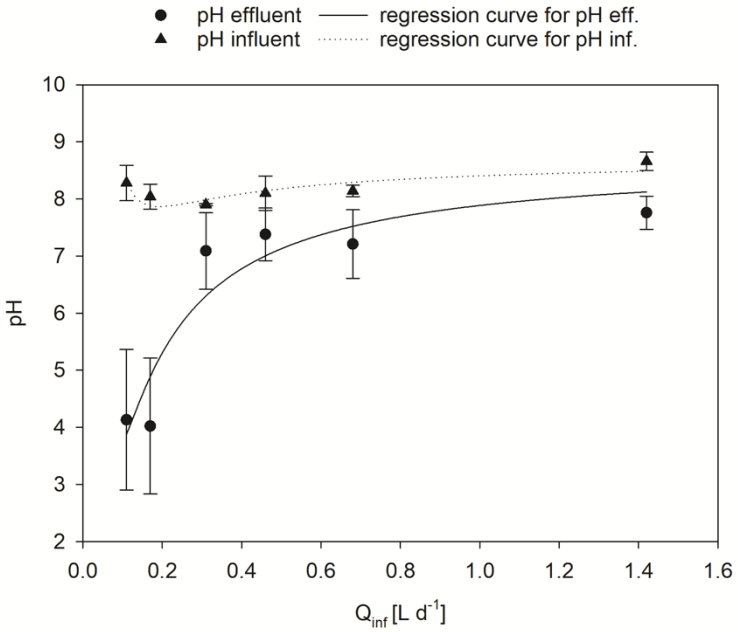

Figure 5. Average influent and effluent pH trend versus the influent flowrate.

Near-acidic pH values in the effluent corresponding to the first Tests may be due to the higher HRT_{des} (e.g., 6.7±0.3 h in Test 1) that allowed protons produced at the anode (pH 2.0±0.7) to pass through the AEM, because of their small size. By reducing the HRT_{des} down to 0.5±0.02 h (Test 6), the faster solution replacement led to a slower pH increase in the

bio-cathode compartment, and to a lower passage of protons through the AEM into the effluent. In addition, the resulting dosage of HCl per m^3 of treated water was significantly reduced (from 109 L m^{-3} to 8.4 L m^{-3}) as the influent flowrate increased, thus implying lower operating costs in the perspective of process scale-up.

3.3 Bacterial community diversity on the bio-cathode of the 3-compartment BES

Cathodic biomass was collected during Test 5. The number of observed ASVs in the bacterial community was 99 and its composition is shown in Figure 6. The most abundant phyla of Bacteria in the biomass were Proteobacteria (44.0%) followed by Actinobacteriota (16.0%), Firmicutes (11.8%), Bacteroidota (10.8%), Planctomycetota (5.1%) and Chloroflexi (4.8%). The other less abundant phyla were all below the 3%, while the unassigned sequences accounted for 1.1% in the composition of bacterial community (Figure 6A). At order level (Figure 6B), the most abundant taxa were Rhizobiales (17.0%), Corynebacteriales (7.4%), and Burkholderiales (6.6%), followed by Xanthomonadales (4.5%), Alteromonadales (4.3%), and Thermomicrobiales (4.2%). At genus level (Figure 6C), the seven most abundant taxa accounted for more than 20% of the total community, including the genera *Rhizobium* (3.9%) and *Bosea* (3.1%) in Rhizobiales, *Mycobacterium* (3.2%) and *Gordonia* (2.4%) in Corynebacteriales, *Fontibacter* (2.6%) in Cytophagales, *Clostridium sensu strictu* (2.4%) in Firmicutes as well as the uncultured JG30-KF-CM45 in Thermomicrobiales (3.2%).

An active role in denitrifying biomass has been previously proposed for several bacteria dominating the bio-cathodic biomass. More specifically, isolates affiliated to Rhizobiales have been proved to denitrify under autotrophic and heterotrophic conditions (Vilar-Sanz et al., 2108), and the genus *Rhizobium* has been implied in denitrification in MFC system for treating saline wastewater (Xu et al., 2019). *Clostridium sensu strictu* has been detected at a

high amount in MEC biomass and suggested to be responsible for autotrophic denitrification in a bioelectrochemically-assisted constructed wetland system (Sotres et al., 2015; Xu et al., 2017). Recently, the genus *Fontibacter* has been found to be enriched after long-term adaptation in a BES for nitrate removal from coke wastewater effluent (Tang et al., 2017) and a species of the genus, isolated from an MFC, has been proved to couple oxidation of organic matter to Fe(III) reduction (Zhang et al., 2013). On the contrary, other dominant populations in the biomass, such as Corynebacteriales, have been less extensively described, and their metabolic role in bioelectrochemical systems is far to be undiscovered.

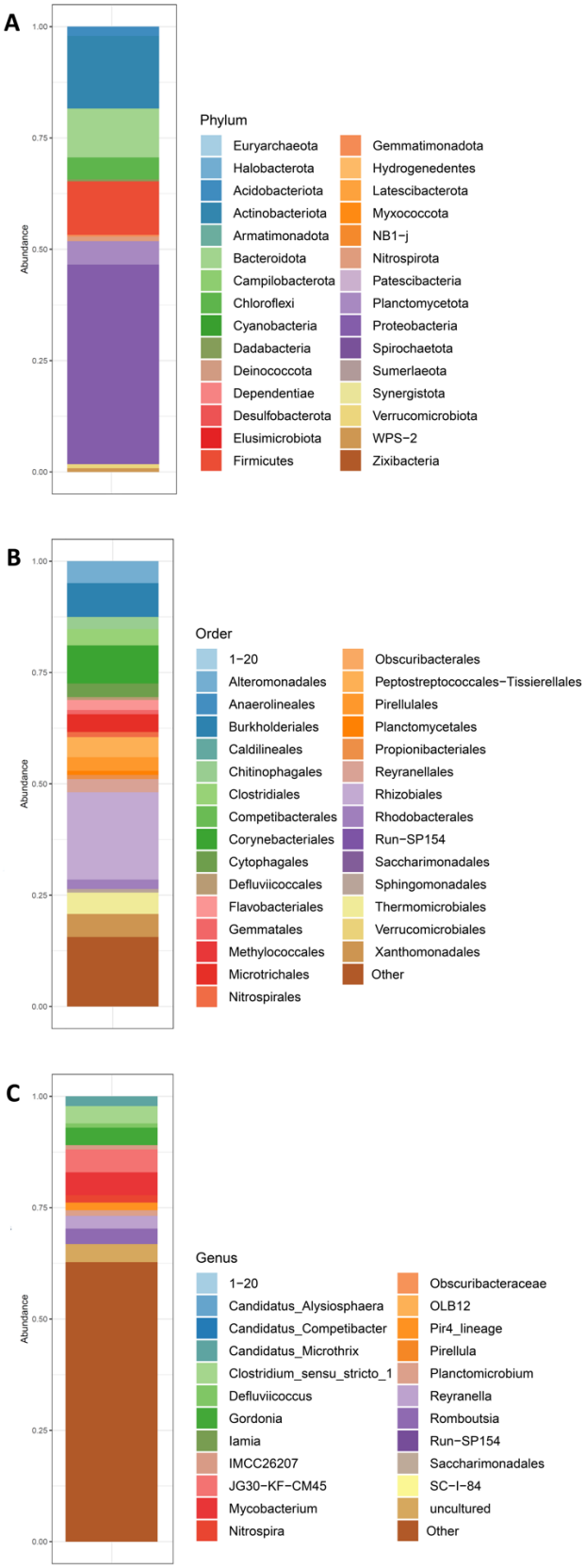

Figure 6. Bacterial community composition of the biofilm formed on the bio-cathode of the 3-compartment bio-electrochemical cells under galvanostatic mode. Bar plots showing the contribution at phylum **(A)** and order **(B)** levels, and the relative abundances of the 30 most abundant genera **(C)**.

3.4 Sustainability perspective on the application of BES for simultaneous denitrification and desalination

In order to move towards scaling up the proposed technology for groundwater treatment, the system must be both technically and economically feasible. For this reason, a preliminary and simplified cost-benefit analysis was carried out comparing the main operational costs associated with the technology and the potential benefits obtained according to experimental data.

The operating costs of a technology depend significantly on the energy consumption of the process. Figure 7 shows the profiles of the specific energy consumption (SEC) per gram of NO_3^--N removed and per volume of water treated as a function of influent flowrate, compared with the trend in N-RR. During the experiment, an improvement of process performance was observed in terms of nitrate removal and SEC, the latter being significantly reduced from $35.2 \cdot 10^{-2} \pm 3.6 \cdot 10^{-2}$ kWh $g^{-1}NO_3^-N_{removed}$ and 6.1±0.4 kWh $m^{-3}_{water\ treated}$ (Test 1) to $5.1 \cdot 10^{-2} \pm 0.7 \cdot 10^{-2}$ kWh $g^{-1}NO_3^-N_{removed}$ and 0.5±0.03 kWh $m^{-3}_{water\ treated}$ (Test 6).

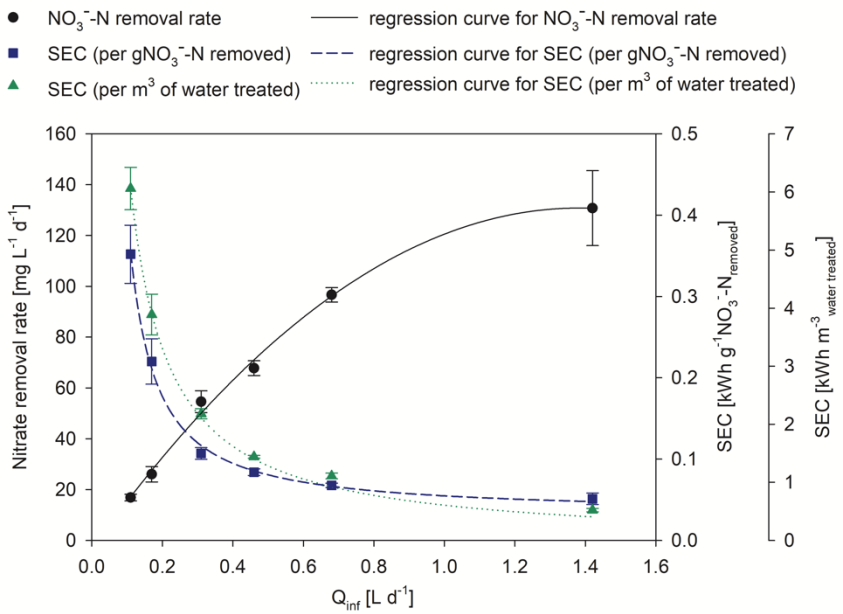

Figure 7. Average trends of SEC per gram of nitrate-nitrogen removed and per volume of water treated, and of N-RR with increasing Q_{inf}.

Pous et al. (2015) reported a list of SECs for various technologies such as bioelectrochemical systems (BES), biofilm electrode reactor (BER), membrane bioreactor (MBR), electrodialysis (ED) and reverse osmosis (RO) (Zhao et al., 2011; Twomey et al., 2010; McAdam and Judd, 2008; Ortiz et al., 2008). Compared to the reported values, the energy consumption per m^3 of treated water was within the range reported for desalination technologies, i.e., electrodialysis and reverse osmosis (0.04 - 2.09 kWh $m^{-3}_{treated\ water}$). The energy consumption per gram of nitrate removed obtained in the present study was in line with those of the technologies reported for nitrate removal, mainly BES and BER ($0.16 \cdot 10^{-2}$ - $7 \cdot 10^{-2}$ kWh $g^{-1}NO_3^-\text{-}N_{removed}$). More specifically, the values obtained in this study are closer to those of BER (i.e., $7 \cdot 10^{-2}$ kWh $g^{-1}NO_3^-\text{-}N_{removed}$), which are based on the application of a potential difference between the electrodes. This type of catalytical operation produces hydrogen in the cathode chamber, which is then used by bacteria to reduce nitrate. In the present study, the current was fixed, and the potential established at the cathode (approximately -1.3 V vs Ag/AgCl) was suitable for hydrogen production. According to Pous et al. (2015), fixing the cathode potential makes it possible to control the reduction of nitrate to the end products and implies less energy consumption. In the present study, however, the aim was not only to remove nitrate but also to reduce the electrical conductivity of groundwater, as well as the production of value-added products (i.e., chlorine). In fact, during the process, part of the chloride accumulated in the solution of the anode compartment is converted into free chlorine (Puggioni et al., 2021). Thus, the energy applied is used to carry out three processes simultaneously with consumption comparable to systems carrying out a single process (i.e., only denitrification or desalination). At the best HRT tested (i.e., 4.9±0.4 h, Test 5), the total cost of energy consumption was as low as 0.23 € m^{-3}, assuming an energy cost of 0.21 € kWh^{-1} (Eurostat, 2021). This value is competitive, considering that

493 Ceballos-Escalera et al. (2022) estimated an operating cost of 0.14 € m^{-3} for the removal
494 of only nitrate using BES.

495 From an economic point of view, the production of chlorine also plays an important role.
496 Chlorine is a disinfectant agent that is highly used in water treatment plants, and its market
497 value is growing significantly due to the rising demand from the agrochemical and
498 pharmaceutical industries. Moreover, the rising demand for water treatment applications
499 combined with increased awareness of better hygiene practices resulting from the impact
500 of the Sars-CoV-2 pandemic will drive the need for chlorine among industrialists.
501 Greaves et al. (2022) demonstrated that Sars-CoV-2 is successfully eliminated by
502 disinfection with free chlorine in both deionised water and wastewater. Web-based
503 chlorine market data show a forecast growth of the chlorine value at a CAGR (compound
504 annual growth rate) between 3.5 and 4.5% for the period 2021-2027.

505 In the present study, up to 0.17 gCl_2 per $gCl^-_{removed}$ were produced, and this production
506 can easily be increased by switching to a continuous operating mode in the anodic
507 chamber or by stripping the chlorine produced. In fact, Puggioni et al. (2021) showed
508 higher production rates at the start of the batch that gradually decreased to a plateau over
509 long periods of operation. Therefore, switching to a continuous operating mode would
510 increase production rates while avoiding chlorine accumulation and excessive
511 concentrations in the anode chamber. Optimising the chlorine capture system seems
512 essential to maximise its production and reduce the contact time with the materials in the
513 bioelectrochemical cell.
514

515 **4. CONCLUSIONS**

516 At higher flowrates (and lower HRT, between 7.3±0.6 and 2.4±0.2 h), an increase in
517 nitrate removal rates up to 131 $mgNO_3^-$-N $L^{-1}d^{-1}$ was observed. At an HRT of 2.4±0.2 h

(Test 6), an effluent nitrate concentration above threshold levels for human consumption (91/767/EU) and the presence of intermediates were observed, indicating a worsening of the denitrifying performance of the system. Desalination performance was reduced in terms of EC-RE (from 77±13% to 12±2%), but the effluent electrical conductivity remained close to the threshold levels for human consumption (98/83/CE). In addition, the bacterial community in the cathodic biomass under galvanostatic mode was dominated by few populations, which were previously demonstrated to have an active role in denitrifying biomass. The tests carried out in the present study demonstrate the economic potential of the proposed technology thanks to the possibility of considerably reducing specific energy consumption while simultaneously increasing denitrification performance. Such a result was achieved by acting on the treated flowrate (i.e., by reducing hydraulic retention times) and not on the reactor volumes, which would imply additional costs in terms of materials and space. Finally, chlorine production represents an enormous potential for possible real application as it would reduce the costs of any on-site disinfection or, in general, an economic return if resold.

ACKNOWLEDGEMENTS

This work was funded through the Fondo di Sviluppo e Coesione 2014-2020, Patto per lo sviluppo della Regione Sardegna - Area Tematica 3 - Linea d' Azione 3.1, "Interventi di sostegno alla ricerca". Project SARdNAF "Advanced Systems for the Removal of Nitrates from Groundwater", ID: RASSR53158. S.P. is a Serra Hunter Fellow (UdG-AG-575) and acknowledges the funding from the ICREA Academia award. LEQUIA has been recognised as a consolidated research group by the Catalan Government (2017-SGR-1552). The authors would like to thank Ms Orietta Masala (CNR-IGAG) for her support with the ICP/OES analysis.

REFERENCES

Alfarrah, N., Walraevens, K., 2018. Groundwater Overexploitation and Seawater Intrusion in Coastal Areas of Arid and Semi-Arid Regions. Water 10, 143. https://doi.org/10.3390/w10020143

Bolyen, E., Rideout, J. R., Dillon, M. R., Bokulich, N. A., Abnet, C. C., Al-Ghalith, G. A., et al.. (2019). Reproducible, interactive, scalable and extensible microbiome data science using QIIME 2. Nature Biotechnology, 37(8), 852–857. 10.1038/s41587-019-0209-9

Callahan, B. J., McMurdie, P. J., Rosen, M. J., Han, A. W., Johnson, A. J. A., & Holmes, S. P. (2016). DADA2: High-resolution sample inference from Illumina amplicon data. Nature Methods, 13(7), 581–583. 10.1038/nmeth.3869

Carrey, R., Ballesté, E., Blanch, A.R., Lucena, F., Pons, P., López, J.M., Rull, M., Solà, J., Micola, N., Fraile, J., Garrido, T., Munné, A., Soler, A., Otero, N., 2021. Combining multi-isotopic and molecular source tracking methods to identify nitrate pollution sources in surface and groundwater. Water Res. 188, 116537. 10.1016/j.watres.2020.11653

Ceballos-Escalera, A., Pous, N., Balaguer, M.D., Puig, S., 2022. Electrochemical water softening as pretreatment for nitrate electro bioremediation. Sci. Total Environ. 806, 150433. 10.1016/j.scitotenv.2021.150433

Ceballos-Escalera, A., Pous, N., Chiluiza-Ramos, P., Korth, B., Harnisch, F., Bañeras, L., Balaguer, M.D., Puig, S., 2021. Electro-bioremediation of nitrate and arsenite polluted groundwater. Water Res. 190, 116748. 10.1016/j.watres.2020.116748

565 Clauwaert, P., Desloover, J., Shea, C., Nerenberg, R., Boon, N., Verstraete, W., 2009.
566 Enhanced nitrogen removal in bio-electrochemical systems by pH control.
567 Biotechnol. Lett. 31, 1537–1543. 10.1007/s10529-009-0048-8
568 Cruz Viggi, C., Tucci, M., Resitano, M., Crognale, S., Di Franca, M.L., Rossetti, S.,
569 Aulenta, F. 2022. Coupling of bioelectrochemical toluene oxidation and
570 trichloroethene reductive dechlorination for single-stage treatment of
571 groundwater containing multiple contaminants. Environmental Science and
572 Ecotechnology 11, 100171. 10.1016/j.ese.2022.100171.
573 Desloover, J., Puig, S., Virdis, B., Clauwaert, P., Boeckx, P., Verstraete, W., Boon, N.,
574 2011. Biocathodic Nitrous Oxide Removal in Bioelectrochemical Systems.
575 Environ. Sci. Technol. 45, 10557–10566. 10.1021/es202047x
576 Electricity price statistics [WWW Document], n.d. URL
577 https://ec.europa.eu/eurostat/statistics-
578 explained/index.php?title=Electricity_price_statistics (accessed 11.29.21).
579 Gounari, C., Skordas, K., Gounaris, A., Kosmidis, D., Karyoti, A., 2014. Seawater
580 Intrusion and Nitrate Pollution in Coastal Aquifer of Almyros – Nea Anchialos
581 Basin, Central Greece 10, 13
582 Greaves, J., Fischer, R.J., Shaffer, M., Bivins, A., Holbrook, M.G., Munster, V.J., Bibby,
583 K., 2022. Sodium hypochlorite disinfection of SARS-CoV-2 spiked in water and
584 municipal wastewater. Sci. Total Environ. 807, 150766.
585 10.1016/j.scitotenv.2021.150766
586 Imoro, A.Z., Mensah, M., Buamah, R., 2021. Developments in the microbial desalination
587 cell technology: A review. Water-Energy Nexus 4, 76,87.
588 10.1016/j.wen.2021.04.002.

589 Janža, M., 2022. Optimisation of well field management to mitigate groundwater
590 contamination using a simulation model and evolutionary algorithm. Sci. Total
591 Environ. 807, 150811. 10.1016/j.scitotenv.2021.150811
592 Jingyu, H., Ewusi-Mensah, D., Norgbey, E., 2017. Microbial desalination cells
593 technology: a review of the factors affecting the process, performance and
594 efficiency. Desalination and Water Treatment. 87, 140–159.
595 10.5004/dwt.2017.21302
596 Kim, Y., Logan, B.E., 2013. Microbial desalination cells for energy production and
597 desalination. Desalination 308, 122–130. 10.1016/j.desal.2012.07.022
598 Klindworth, A., Pruesse, E., Schweer, T., Peplies, J., Quast, C., Horn, M., & Glöckner,
599 F. O. (2013). Evaluation of general 16S ribosomal RNA gene PCR primers for
600 classical and next-generation sequencing-based diversity studies. Nucleic Acids
601 Research, 41(1), 1–11. https://doi.org/10.1093/nar/gks808
602 Kwon, E., Park, J., Park, W.-B., Kang, B.-R., Woo, N.C., 2021. Nitrate contamination of
603 coastal groundwater: Sources and transport mechanisms along a volcanic aquifer.
604 Sci. Total Environ. 768, 145204. 10.1016/j.scitotenv.2021.145204
605 Li, Chen, Xie, Liu, Xiong, 2019. Bioelectrochemical Systems for Groundwater
606 Remediation: The Development Trend and Research Front Revealed by
607 Bibliometric Analysis. Water 11, 1532. 10.3390/w11081532
608 Liu, J., Gao, Z., Wang, Z., Xu, X., Su, Q., Wang, S., Qu, W., Xing, T., 2020.
609 Hydrogeochemical processes and suitability assessment of groundwater in the
610 Jiaodong Peninsula, China. Environ. Monit. Assess. 192, 384. 10.1007/s10661-
611 020-08356-5

612 Luo, H., Xu, P., Jenkins, P.E., Ren, Z., 2012. Ionic composition and transport mechanisms
613 in microbial desalination cells. J. Membr. Sci. 409–410, 16–23.
614 https://doi.org/10.1016/j.memsci.2012.02.059

615 McAdam, E.J., Judd, S.J., 2008. Immersed membrane bioreactors for nitrate removal
616 from drinking water: Cost and feasibility. Desalination 231, 52–60.
617 10.1016/j.desal.2007.11.038

618 Oksanen, J., Blanchet, F. G., Friendly, M., Kindt, R., Legendre, P., McGlinn, D., et al.
619 (2019). Vegan. Community Ecology Package.

620 Ortiz, J., Exposito, E., Gallud, F., Garciagarcia, V., Montiel, V., Aldaz, A., 2008.
621 Desalination of underground brackish waters using an electrodialysis system
622 powered directly by photovoltaic energy. Sol. Energy Mater. Sol. Cells 92, 1677–
623 1688. 10.1016/j.solmat.2008.07.020

624 Patil, S., Harnisch, F., Schröder, U., 2010. Toxicity Response of Electroactive Microbial
625 Biofilms-A Decisive Feature for Potential Biosensor and Power Source
626 Applications. ChemPhysChem 11, 2834–2837. 10.1002/cphc.201000218

627 Paulson, J. N., Colin Stine, O., Bravo, H. C., & Pop, M. (2013). Differential abundance
628 analysis for microbial marker-gene surveys. Nature Methods, 10(12), 1200–1202.
629 10.1038/nmeth.2658

630 Pous, N., Balaguer, M.D., Colprim, J., Puig, S., 2018. Opportunities for groundwater
631 microbial electro-remediation. Microb. Biotechnol. 11, 119–135. 10.1111/1751-
632 7915.12866

633 Pous, N., Puig, S., Balaguer, M.D., Colprim, J., 2017. Effect of hydraulic retention time
634 and substrate availability in denitrifying bioelectrochemical systems. Environ.
635 Sci. Water Res. Technol. 3, 922–929. 10.1039/C7EW00145B

636 Pous, N., Puig, S., Dolors Balaguer, M., Colprim, J., 2015. Cathode potential and anode
637 electron donor evaluation for a suitable treatment of nitrate-contaminated
638 groundwater in bioelectrochemical systems. Chem. Eng. J. 263, 151–159.
639 10.1016/j.cej.2014.11.002
640 Pous, N., Puig, S., Coma, M., Balaguer, M.D., Colprim, J., 2013. Bioremediation of
641 nitrate-polluted groundwater in a microbial fuel cell: Bioremediation of nitrate-
642 polluted groundwater in a microbial fuel cell. J. Chem. Technol. Biotechnol. 88,
643 1690–1696. https://doi.org/10.1002/jctb.4020
644 Puggioni, G., Milia, S., Dessì, E., Unali, V., Pous, N., Balaguer, M.D., Puig, S., Carucci,
645 A., 2021. Combining electro-bioremediation of nitrate in saline groundwater with
646 concomitant chlorine production. Water Res. 206, 117736.
647 10.1016/j.watres.2021.117736
648 Puig, S., Coma, M., Desloover, J., Boon, N., Colprim, J., Balaguer, M.D., 2012.
649 Autotrophic Denitrification in Microbial Fuel Cells Treating Low Ionic Strength
650 Waters. Environ. Sci. Technol. 46, 2309–2315.
651 https://doi.org/10.1021/es2030609
652 Quast, C., Pruesse, E., Yilmaz, P., Gerken, J., Schweer, T., Yarza, P., et al. (2013). The
653 SILVA ribosomal RNA gene database project: improved data processing and
654 web-based tools. Nucleic Acids Res. 41, 590–596. 10.1093/nar/gks1219
655 Rahman, S., Jafary, T., Al-Mamun, A., Baawain, M.S., Choudhury, M.R., Alhaimali, H.,
656 Siddiqi, S.A., Dhar, B.R., Sana, A., Lam, S.S., Aghbashlo, M., Tabatabaei, M.,
657 2021. Towards upscaling microbial desalination cell technology: A
658 comprehensive review on current challenges and future prospects. J. Clean. Prod.
659 288, 125597. https://doi.org/10.1016/j.jclepro.2020.125597

660 Ramírez-Moreno, M., Rodenas, P., Aliaguilla, M., Bosch-Jimenez, P., Borràs, E.,
661 Zamora, P., Monsalvo, V., Rogalla, F., Ortiz, J.M., Esteve-Núñez, A., 2019.
662 Comparative Performance of Microbial Desalination Cells Using Air Diffusion
663 and Liquid Cathode Reactions: Study of the Salt Removal and Desalination
664 Efficiency. Front. Energy Res. 7, 135. 10.3389/fenrg.2019.00135
665 Serio, F., Miglietta, P.P., Lamastra, L., Ficocelli, S., Intini, F., De Leo, F., De Donno, A.,
666 2018. Groundwater nitrate contamination and agricultural land use: A grey water
667 footprint perspective in Southern Apulia Region (Italy). Sci. Total Environ. 645,
668 1425–1431. 10.1016/j.scitotenv.2018.07.241
669 Sevda, S., Yuan, H., He, Z., Abu-Reesh, I.M., 2015. Microbial desalination cells as a
670 versatile technology: Functions, optimisation and prospective. Desalination 371,
671 9–17. 10.1016/j.desal.2015.05.021
672 Sotres, A., Cerrillo, M., Viñas, M., Bonmatí, A., 2015. Nitrogen recovery from pig slurry
673 in a two-chambered bioelectrochemical system. Bioresource Technology, 194,
674 373–382. 10.1016/j.biortech.2015.07.036
675 Tang, R., Wu, D., Chen, W., Feng, C., Wei, C., 2017. Biocathode denitrification of coke
676 wastewater effluent from an industrial aeration tank: Effect of long-term
677 adaptation. Biochemical Engineering Journal, 125, 151–160.
678 10.1016/j.bej.2017.05.022
679 Troudi, N., Hamzaoui-Azaza, F., Tzoraki, O., Melki, F., Zammouri, M., 2020.
680 Assessment of groundwater quality for drinking purpose with special emphasis on
681 salinity and nitrate contamination in the shallow aquifer of Guenniche (Northern
682 Tunisia). Environ. Monit. Assess. 192, 641. 10.1007/s10661-020-08584-9

683 Tucci, M., Cruz-Viggi, C., Resitano, M., Matturro, B., Crognale, S., Pietrini, I., Rossetti,
684 S., Harnisch, F., Aulenta, F., 2021. Simultaneous removal of hydrocarbons and
685 sulfate from groundwater using a “bioelectric well”. Electrochimica Acta 388,
686 138636. 10.1016/j.electacta.2021.138636.

687 Twomey, K.M., Stillwell, A.S., Webber, M.E., 2010. The unintended energy impacts of
688 increased nitrate contamination from biofuels production. J Env. Monit 12, 218–
689 224. 10.1039/B913137J

690 Vilà-Rovira, A., Puig, S., Balaguer, M.D., Colprim, J., 2015. Anode hydrodynamics in
691 Bioelectrochemical Systems 9. RSC Advances.
692 https://pubs.rsc.org/en/Content/ArticleLanding/2015/RA/c5ra11995b

693 Vilar-Sanz, A., Pous, N., Puig, S., Balaguer, M. D., Colprim, J., Bañeras, L., 2018.
694 Denitrifying nirK-containing alphaproteobacteria exhibit different electrode
695 driven nitrite reduction capacities. Bioelectrochemistry, 121, 74–83.
696 10.1016/j.bioelechem.2018.01.007

697 Virdis, B., Rabaey, K., Yuan, Z., Keller, J., 2008. Microbial fuel cells for simultaneous
698 carbon and nitrogen removal. Water Res. 42, 3013–3024.
699 10.1016/j.watres.2008.03.017

700 Virdis, B., Rabaey, K., Yuan, Z., Rozendal, R.A., Keller, J., 2009. Electron Fluxes in a
701 Microbial Fuel Cell Performing Carbon and Nitrogen Removal. Environ. Sci.
702 Technol. 43, 5144–5149. https://doi.org/10.1021/es8036302

703 Wang, C., Dong, J., Hu, W., Li, Y., 2021. Enhanced simultaneous removal of nitrate and
704 perchlorate from groundwater by bioelectrochemical systems (BESs) with
705 cathodic potential regulation. Biochem. Eng. J. 173, 108068.
706 10.1016/j.bej.2021.108068

Wang, X., Aulenta, F., Puig, S., Esteve-Núñez, A., He, Y., Mu, Y., Rabaey, K., 2020. Microbial electrochemistry for bioremediation. Environ. Sci. Ecotechnology 1, 100013. 10.1016/j.ese.2020.100013

Xu, D., Xiao, E., Xu, P., Zhou, Y., He, F., Zhou, Q., … Wu, Z., 2017. Performance and microbial communities of completely autotrophic denitrification in a bioelectrochemically-assisted constructed wetland system for nitrate removal. Bioresource Technology, 228, 39–46. 10.1016/j.biortech.2016.12.065

Xu, F., Ouyang, D. long, Rene, E. R., Ng, H. Y., Guo, L. ling, Zhu, Y. jie, Kong, Q., 2019. Electricity production enhancement in a constructed wetland-microbial fuel cell system for treating saline wastewater. Bioresource Technology, 288(May), 121462. 10.1016/j.biortech.2019.121462

Zhang, Y., Angelidaki, I., 2013. A new method for in situ nitrate removal from groundwater using submerged microbial desalination–denitrification cell (SMDDC). Water Res. 47, 1827–1836. 10.1016/j.watres.2013.01.005

Zhang, J., Yang, G. Q., Zhou, S., Wang, Y., Yuan, Y., & Zhuang, L., 2013. *Fontibacter ferrireducens* sp. nov., an Fe(III)-reducing bacterium isolated from a microbial fuel cell. International Journal of Systematic and Evolutionary Microbiology, 63(PART3), 925–929. 10.1099/ijs.0.040998-0

Zhao, Y., Feng, C., Wang, Q., Yang, Y., Zhang, Z., Sugiura, N., 2011. Nitrate removal from groundwater by cooperating heterotrophic with autotrophic denitrification in a biofilm–electrode reactor. J. Hazard. Mater. 192, 1033–1039. 10.1016/j.jhazmat.2011.06.008